

Article

Deformation Measurements of Helicopter Rotor Blades Using a Photogrammetric System

Chenglin Zuo *, Jun Ma, Chunhua Wei, Tingrui Yue and Jin Song

China Aerodynamics Research and Development Center, Low Speed Aerodynamics Institute, Mianyang 621000, China; majunttt@sina.com (J.M.); weichunhua@cardc.cn (C.W.); yuetingrui@cardc.cn (T.Y.); songjin830131@sina.com (J.S.)

* Correspondence: zuochenglin@cardc.cn

Abstract: As an important part of the helicopter, the rotor directly affects flight safety and flight quality. Knowledge of the rotor dynamic behaviors is significant for validating and optimizing the performance of the helicopter rotor system. In this study, a photogrammetric system, based on 3D point tracking and stereo photogrammetry technology, is presented to solve the full-field dynamic motion and deformation parameters of rotating blades by identifying the retro-reflective targets arranged on the rotor. The photogrammetric system is demonstrated in the wind tunnel tests of a 2 m-diameter model rotor, conducted at the 5.5 m × 4 m Aeroacoustic Wind Tunnel of the China Aerodynamics Research and Development Center (CARD C). With the targets attached on the special hat installed directly over the rotor hub, a unified rotor coordinate system, that was stationary with respect to the rotor, could be established at any measuring instant. Therefore, by transforming the 3D coordinates of all measured targets to the rotor coordinate system, the blade displacements and deformations at different test conditions could be calculated consistently. Experimental results from current study were compared to simulation results calculated by the comprehensive analytical model of rotorcraft aerodynamics and dynamics (CAMRAD), which shows quite good agreements.

Keywords: rotor blade; point tracking; stereo photogrammetry; displacements and deformations



Citation: Zuo, C.; Ma, J.; Wei, C.; Yue, T.; Song, J. Deformation Measurements of Helicopter Rotor Blades Using a Photogrammetric System. *Photonics* **2022**, *9*, 466. <https://doi.org/10.3390/photonics9070466>

Received: 29 May 2022

Accepted: 30 June 2022

Published: 3 July 2022

Publisher's Note: MDPI stays neutral with regard to jurisdictional claims in published maps and institutional affiliations.



Copyright: © 2022 by the authors. Licensee MDPI, Basel, Switzerland. This article is an open access article distributed under the terms and conditions of the Creative Commons Attribution (CC BY) license (<https://creativecommons.org/licenses/by/4.0/>).

1. Introduction

Blade deformation measurements play an important role in the validation and improvement of the helicopter rotor. It is used to resolve the rotor blade shape and position, including blade root pitch, flap, lag and elastic deformation. When combined with blade airloads and wake measurements, a comprehensive dataset is formed that directly relates the rotor performance to the physical properties of the flow, thereby providing a great quantity of information for the continued design and aerodynamic improvements of the rotor system.

The wind tunnel test is an important tool to measure the blade deformation of the helicopter rotor. Typically, experimental testing primarily makes use of strain gauges as measurement sensors to relate local strains and blade deformation [1,2]. However, due to blade size constraints, the number of strain gauges that can be arranged is usually insufficient. Additionally, strain gauges have a significant marginal cost, which makes them an expensive solution when lots of acquisition points are required. Moreover, since they require complex wiring, positioning and gluing, the aerodynamic shape of the blades may be deteriorated.

Due to these limitations, optical techniques are gradually used to measure the rotor blade deformation. These techniques are able to provide fairly robust and accurate measurements in a non-contact way, along with the additional benefits of reduced fabrication difficulty and costs [3]. In [4,5], Fleming et al. demonstrated the capability of projection moiré interferometry (PMI) to measure azimuthal variations of rotor blade deformation at different advanced ratios, in or out of fuselage influence. This study was extended to

the test of a model-scale rotor in the NASA Langley 14×22 feet subsonic wind tunnel hover facility [6]. In [7–9], Schneider et al. utilized stereo photogrammetry for the first time to successfully measure the blade positions and deformation at the German-Dutch Wind Tunnel. This technique allows an accurate reconstruction of the blade shape from a number of digital photos taken freehand from different positions and orientations. A triangulation process, based on the correlation of the digital pictures, yields 3D coordinates of designated reference points located on the blades. Later, in [10–13], stereo photogrammetry was employed to measure the displacements and deformations of full-scale UH-60A airloads rotor at various advance ratios, thrust coefficients and drive shaft angles. In the experiments, a number of circular retro-reflective targets were installed at specific locations of each blade, and the experimental results closely matched the design parameters. Analogously, in [14], Straub et al. applied stereo photogrammetry to measure the displacements of a full-scale Boeing SMART active flap rotor at forward flight conditions. Instead of circular targets, Zuo et al. [15,16] applied coded targets arranged on the blades, which could be directly identified according to their encoding information. By using stereo photogrammetry, they achieved displacement and deformation measurements of a 2 m diameter rotor at hover flight conditions. Similarly, Bernardini et al. [17] used photogrammetry to identify the structural characterization of two different blades. In addition, stereoscopic digital image correlation (DIC) has also been widely used to measure the blade deformation of helicopter rotor [18–24]. By spraying a high-contrast random speckle pattern on the rotor blades, in conjunction with photogrammetry, this approach can achieve full-field and continuous measurements.

In this paper, a photogrammetric system is proposed to realize the full-field blade deformation measurements of a 2 m-diameter model rotor in the wind tunnel test. Two main objectives have driven this work: (i) to develop a non-contact approach for the full-field deformation measurements of rotating blades, (ii) to assess its effectiveness and accuracy in real-world applications, such as wind tunnel tests.

2. Experimental Setup

2.1. Experimental Facilities

Experiments were carried out in the $5.5 \text{ m} \times 4 \text{ m}$ Aeroacoustic Wind Tunnel at CARDC. It is a low-speed, low-turbulence, single close circuit wind tunnel, driven by a 12,500 kW variable-speed electric motor. It has two replaceable test sections, including the open test section and the closed test section. In this study, experimental tests were conducted in the open test section, primarily because it allows the photogrammetric system to be installed outside the freestream without any obstruction. The minimum and maximum test section velocities are 8 m/s and 100 m/s, respectively, and the turbulence level is below 0.2%.

Figure 1 shows an overview of the experimental setup. The rotor test stand, driven by a 65 kW electric motor, was supported by a steel base, making the center of the rotor disk plane aligned with the center line of the wind tunnel. The distance of the rotor from the floor was about 8 m. The rated speed of the rotor test stand was 2072 rpm, with the control accuracy better than 1‰. The shaft angle could be varied between -15° and $+10^\circ$, while the collective pitch angle could be varied between 0° and $+15^\circ$, both of which obtained the control accuracy better than 0.1° . The configuration of the rotor hub was hingeless. The rotor was equipped with four blades and had a rotating radius of 1 m. The blade had a cross-sectional shape of NACA23012 airfoil with a chord of $C = 60 \text{ mm}$ and a negative linear twist of -8° . Additionally, a special hat with a 80 mm diameter disk in the center was mounted on the rotor hub. The axis of the hat coincided with that of the rotor shaft. To encompass the full range of rotor motion, the photogrammetric system was installed on the top of a huge portal frame, with 4 m above the rotor.

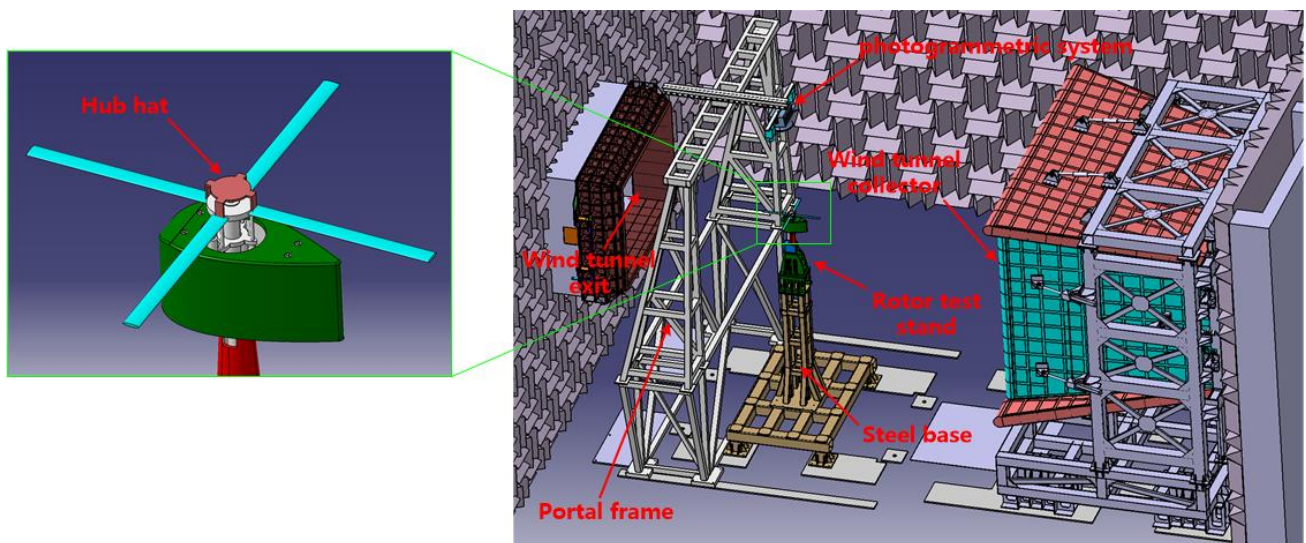


Figure 1. Overview of the experimental setup in the 5.5 m × 4 m Aeroacoustic Wind Tunnel at CARDC.

2.2. Photogrammetric System

Figure 2 illustrates the structure of the photogrammetric system. With the TTL signals from the rotor shaft encoder, the two high-speed cameras were triggered simultaneously to capture the transient images of the rotor blades at different azimuth angles. The LED light source was used to provide enough illumination for the short-exposure imaging of the cameras.

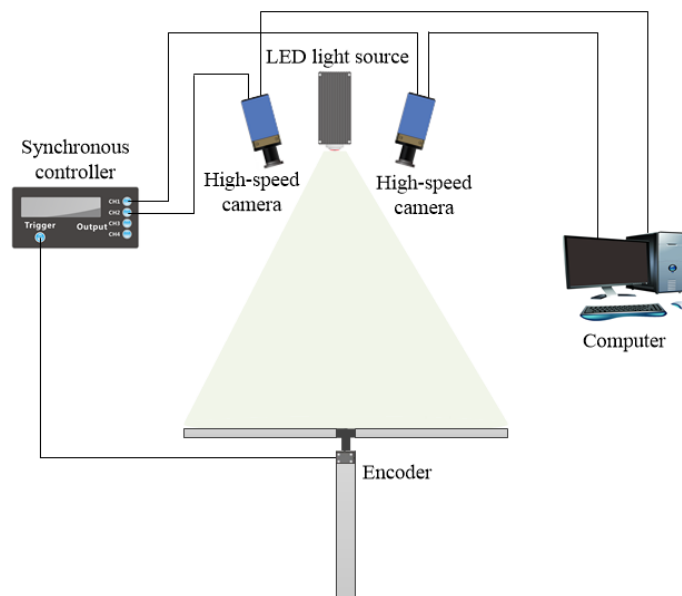


Figure 2. Structure of the photogrammetric system.

The two cameras used in this study have the 12-bit CMOS sensors and can provide a full frame resolution of 2048×2048 pixel at the maximum frame rate of 1080 fps, with the minimum exposure time of $2.7 \mu\text{s}$. Nikon 35 mm f/1.8 G ED lens were configured for the two cameras to cover the full rotating range of rotor blades. The LED light source had the maximum output power of 1500 W. Figure 3 shows the field installed photogrammetric system in the experiments.

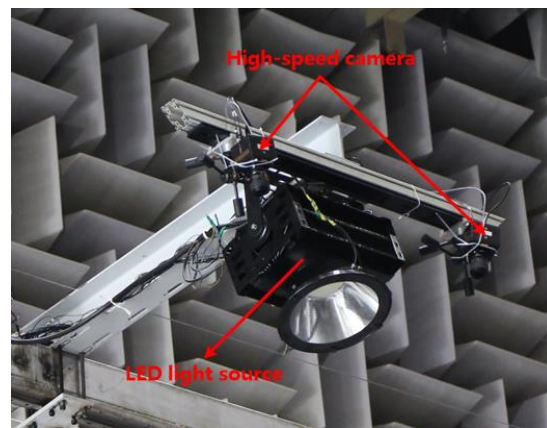


Figure 3. Installed photogrammetric system in the experiments.

2.3. Retro-Reflective Targets

Before the experiments, fifty-two 20 mm diameter retro-reflective targets, two per radial location, were arranged on one blade, covering the blade span from approximately $r/R = 0.23$ to 0.98. In both chordwise and spanwise directions of the blade, the distance between two adjacent targets was 30 mm. In addition, an 80 mm diameter retro-reflective target, with two black targets on it, was also arranged on the hub hat, just covering its disk completely. Both of the two black targets had a diameter of 20 mm. Figure 4 illustrates the distribution of the blade and hub targets, while Figure 5 shows their actual arrangement on the rotor.

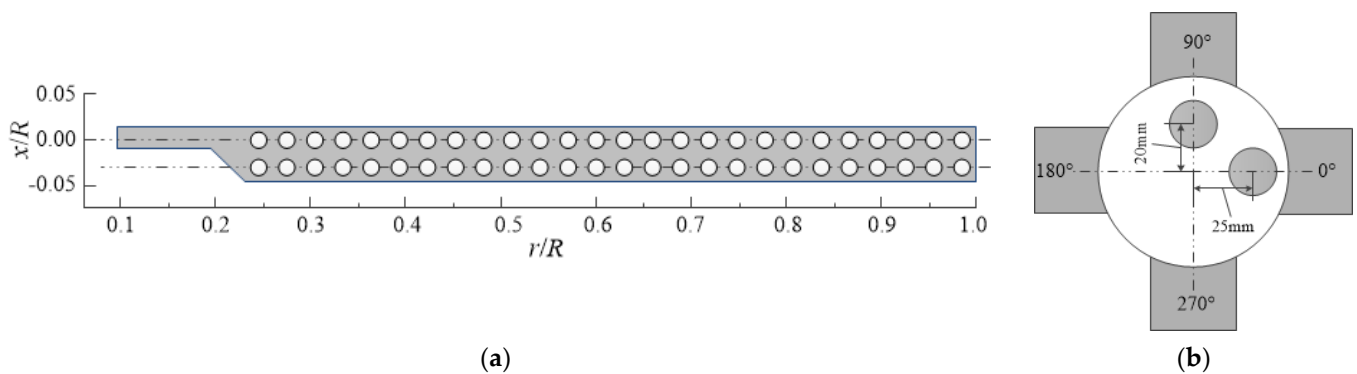


Figure 4. Distribution of (a) the blade targets and (b) the hub targets.

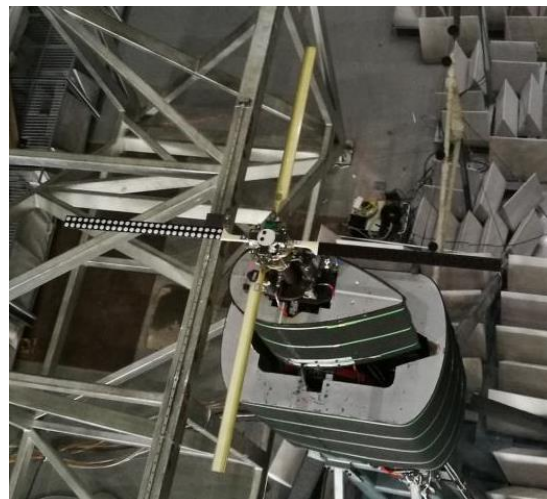


Figure 5. Arrangement of the blade and hub targets.

3. Photogrammetry

Photogrammetry is an innovative, non-contacting measurement technique that allows an accurate reconstruction of the 3D shape of an object from a number of digital images taken from different positions and orientations. The object is reconstructed through the knowledge of the positions of a set of targets pasted on its surface. Figure 6 illustrates the photogrammetry principle. By recognizing and triangulating the targets in the images captured by at least two cameras, the 3D coordinates of the targets in the real world can be calculated.

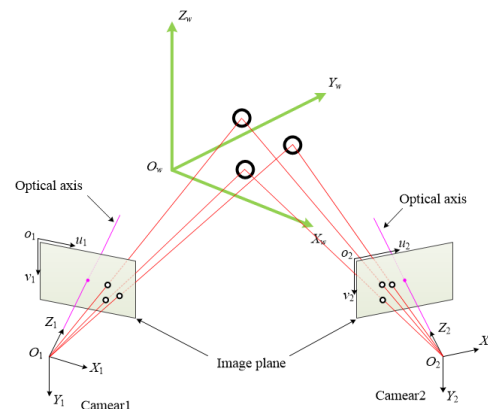


Figure 6. The photogrammetry principle.

3.1. Calibration

A calibration procedure was performed to determine the internal and external parameters for the cameras that relate a 3D object to its two-dimensional images. The internal parameters define the geometric and the optical characteristics of the cameras, while the external parameters describe the rotational and translational information of an image coordinate system with respect to a predefined global coordinate system. Additionally, the distortion parameters of the cameras were also determined through the calibration, which could be used to correct the image distortions.

In this study, a checkerboard plate with a size of 1400 mm × 1000 mm was used for calibration. It contains 15 × 11 black and white grids, while each grid has a size of 80 mm × 80 mm. During calibration, a series of images of the calibration plate were captured by both cameras. For each set of images, the locations of the checkerboard corners on the calibration plate were identified, and their positions were used to calculate, using a pinhole model, the internal and external parameters and image distortion coefficients. Figure 7 shows the examples of calibration images taken by camera 1 and camera 2, while Table 1 shows the calibration results.

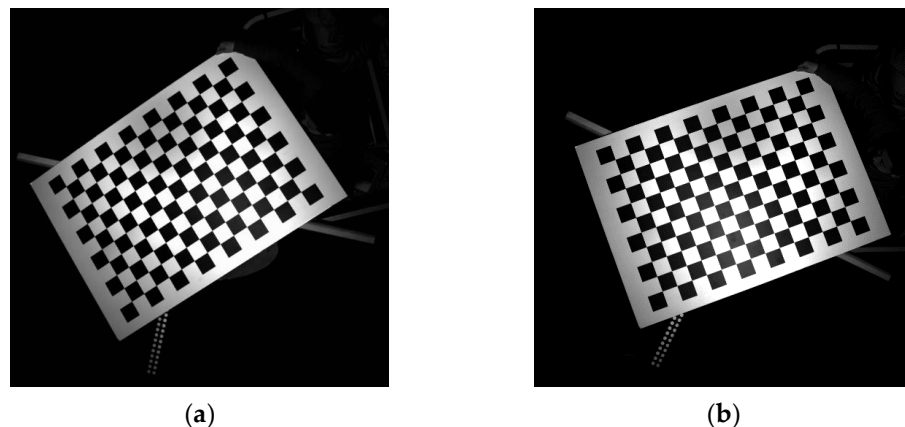


Figure 7. Examples of calibration images taken by (a) camera 1 and (b) camera 2.

Table 1. Calibration results.

Calibration Parameters	Camera 1	Camera 2
Equivalent focal length (f_x, f_y)	(3481.902, 3481.744)	(3474.916, 3474.299)
Principal point (x_0, y_0)	(1022.782, 1040.829)	(1020.625, 1004.494)
skewness coefficient γ	0	0
Radial Distortion Coefficients (k_1, k_2)	(−0.099, 0.107)	(−0.096, 0.058)
Rotation matrix R	$\begin{pmatrix} 1 & 0 & 0 \\ 0 & 1 & 0 \\ 0 & 0 & 1 \end{pmatrix}$	$\begin{pmatrix} 0.936 & -0.228 & -0.266 \\ 0.226 & 0.973 & -0.040 \\ 0.268 & -0.022 & 0.963 \end{pmatrix}$
Translation vector T	(0 0 0)	(−1043.223 114.493 119.592)

3.2. Target Detection, Location and Recognition

Each set of images was processed to detect, locate and recognize the targets on the rotor blade and hub hat. First, image edges were extracted by using the classic edge detection operator, the Canny algorithm. Since the geometry of the targets could be known from the first image of the sequence and did not change significantly, the non-target edges in the image sequence were automatically eliminated with shape and perimeter constraints, while only the target edges were retained. Then, by using least squares ellipse fitting on the edges of each target, the sub-pixel image coordinates of their centroids could be obtained respectively, thereby achieving accurate target location. Figure 8 shows the process of target detection and location.

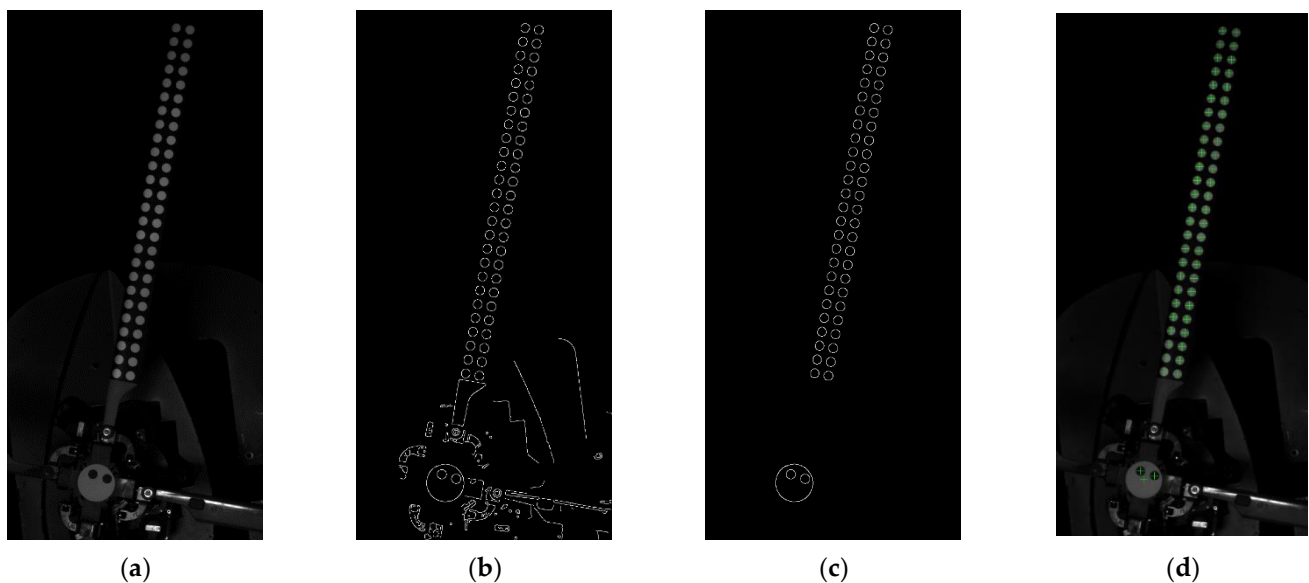


Figure 8. Target detection and location. (a) An example image. (b) Image edges extraction. (c) Target detection. (d) Target location.

After all targets were detected and located, a recognition algorithm was performed to match them in the images synchronously captured by the two cameras. Since the targets were arranged on the rotor regularly, they could be effectively identified based on their positions. First, the large hub target was identified with its different diameter from others, which had been obtained by least-squares ellipse fitting on its edge during the target locating process. Therefore, the rotor hub center could be determined with the centroid of the large hub target. Then, the distances of all other targets from the hub center were computed, based on which the two black hub targets and the blade targets along the radial direction were distinguished. For the targets on the same radial location, identification was completed with their clockwise positions with respect to the hub center. Finally, depending on the recognition results, all targets were numbered, shown in Figure 9, thus resulting in exact target matching.



Figure 9. Numbering of all targets on the rotor.

3.3. Rotor Coordinate System

Although the photogrammetric system was installed outside the wind tunnel freestream, the airflow produced by the high-speed rotation of the rotor still might cause its vibrations. In addition, the rotor test stand itself might also vibrate during rotor rotation. All these potential problems will cause non-negligible influence on the measurement, and finally introduce considerable errors to the results. In this study, based on the targets on the hub hat, a unified rotor coordinate system was established, which took the hub center as the origin and the hub hat plane, fitted by the measured positions of hub targets using least squares, as XY plane, illustrated in Figure 10. For the instantaneously measured blade targets, their 3D coordinates were transformed to the rotor coordinate system. Therefore, the blade displacements and deformations at different test conditions could be calculated consistently. Additionally, since the rotor coordinate system was stationary with respect to the rotor, measurements would not be disturbed by the vibrations of the photogrammetric system or the rotor, thus leading to accurate results.

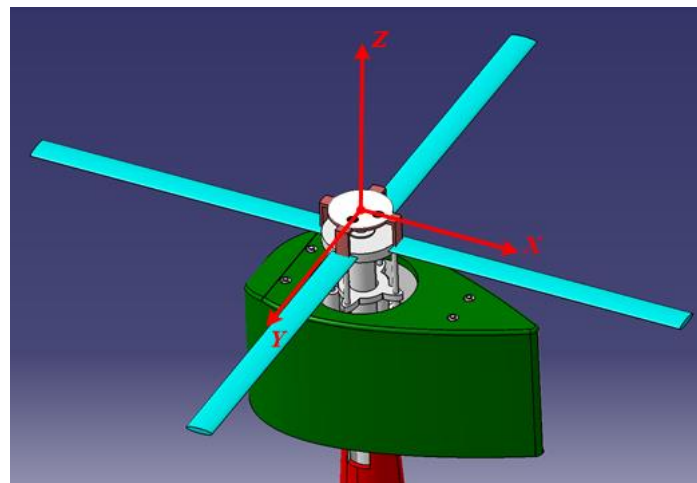


Figure 10. Rotor coordinate system.

4. Results and Discussion

In this study, blade deformations in the hover flight were measured continuously throughout the experiments. Five test conditions were performed, including: $N = 1858$ rpm, $\theta = 0^\circ, 2^\circ, 4^\circ, 6^\circ, 8^\circ$. Additionally, the hover flight condition with $N = 50$ rpm and $\theta = 0^\circ$ was also measured, which provided a reference to calculate the displacements and deformations of the rotor blade at different test conditions.

Figure 11 shows the 3D reconstruction results of the rotor blade measured at the same azimuth location with five different collective pitch angles. As the collective pitch angle increased, the blade raised gradually. Compared to the blade root, the blade tip suffered from greater aerodynamic loads, and thus notable displacements and deformations could be observed there.

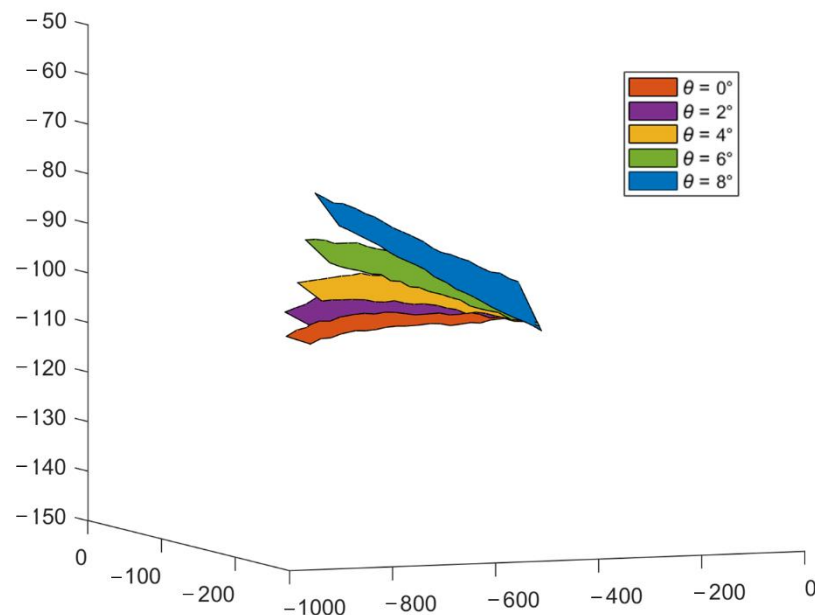


Figure 11. The 3D reconstruction results of the rotor blade measured at the same azimuth location with five different collective pitch angles in hover flight.

Figure 12a quantitatively shows the average displacements of the rotor blade at its eight radial locations. As the collective pitch angle increased, displacements of the blade root were quite small, while the blade tip suffered from the greatest displacements. Besides, the growth of blade displacements along its radial direction also became faster with the

increase of the collective pitch angle, which indicated that blade deformations appeared. Figure 12b shows the detailed displacements of the blade tip. It can be seen that the flapping displacements of the blade tip were generally stable, but still with some fluctuations. Furthermore, the experimental results were compared to the computational structure dynamics (CSD) results calculated with the CAMRAD software, shown in Figure 13. The two results obtained a perfect agreement with only a slight offset.

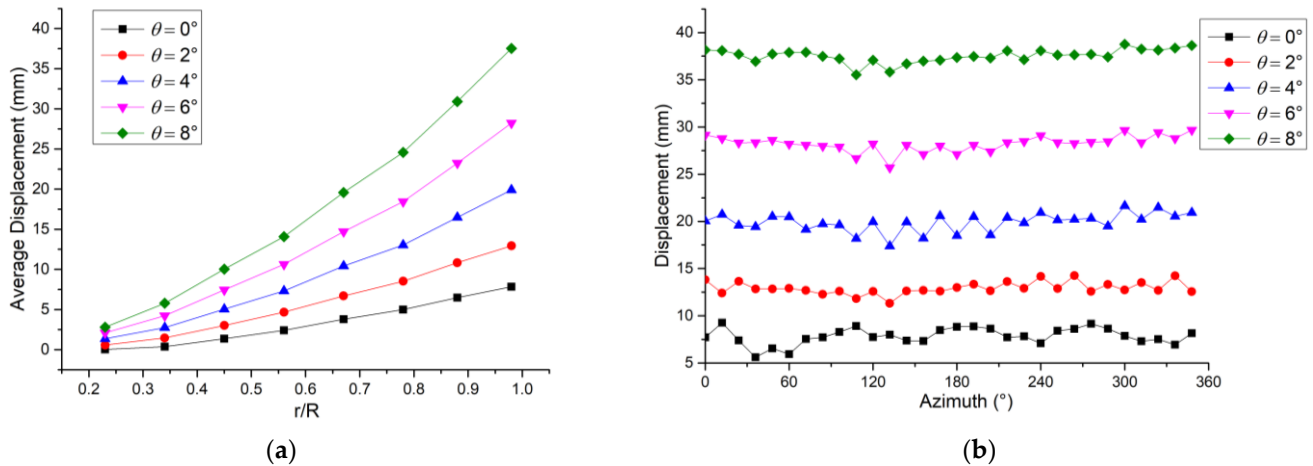


Figure 12. (a) Average displacements at eight radial locations of the rotor blade. (b) Blade tip displacements at five collective pitch angles.

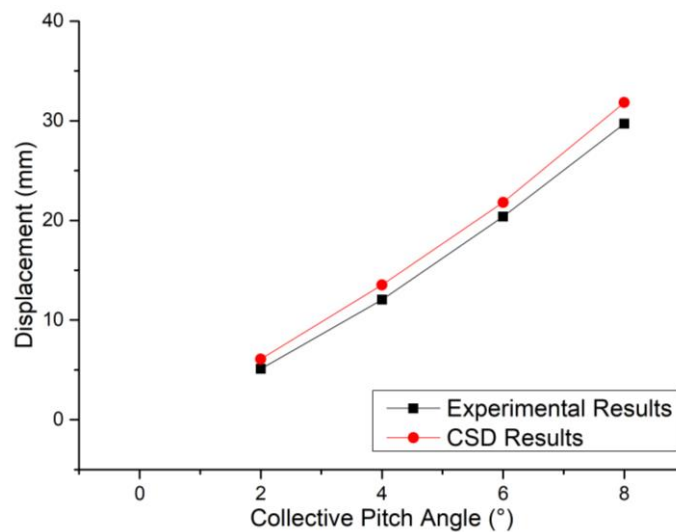


Figure 13. Comparison of the average blade tip displacements between experimental and CSD results.

Figure 14 shows the average flap bending deformations of the rotor blade over its full rotating range at five collective pitch angles. It can be observed that the blade tip always suffered from the greatest deformations. The larger the collective pitch angle, the greater the blade deformations. Additionally, the blade deformations increased gradually along its radial direction, which agreed with the blade displacement changes well. Figure 15 shows the average blade deformations at its eight radial locations further. Similar to the blade displacement changes, the blade deformations became greater as the collective pitch angle increased. In Figure 16, the blade deformations over its full rotating range with the collective pitch angle of $\theta = 8^\circ$ are shown.

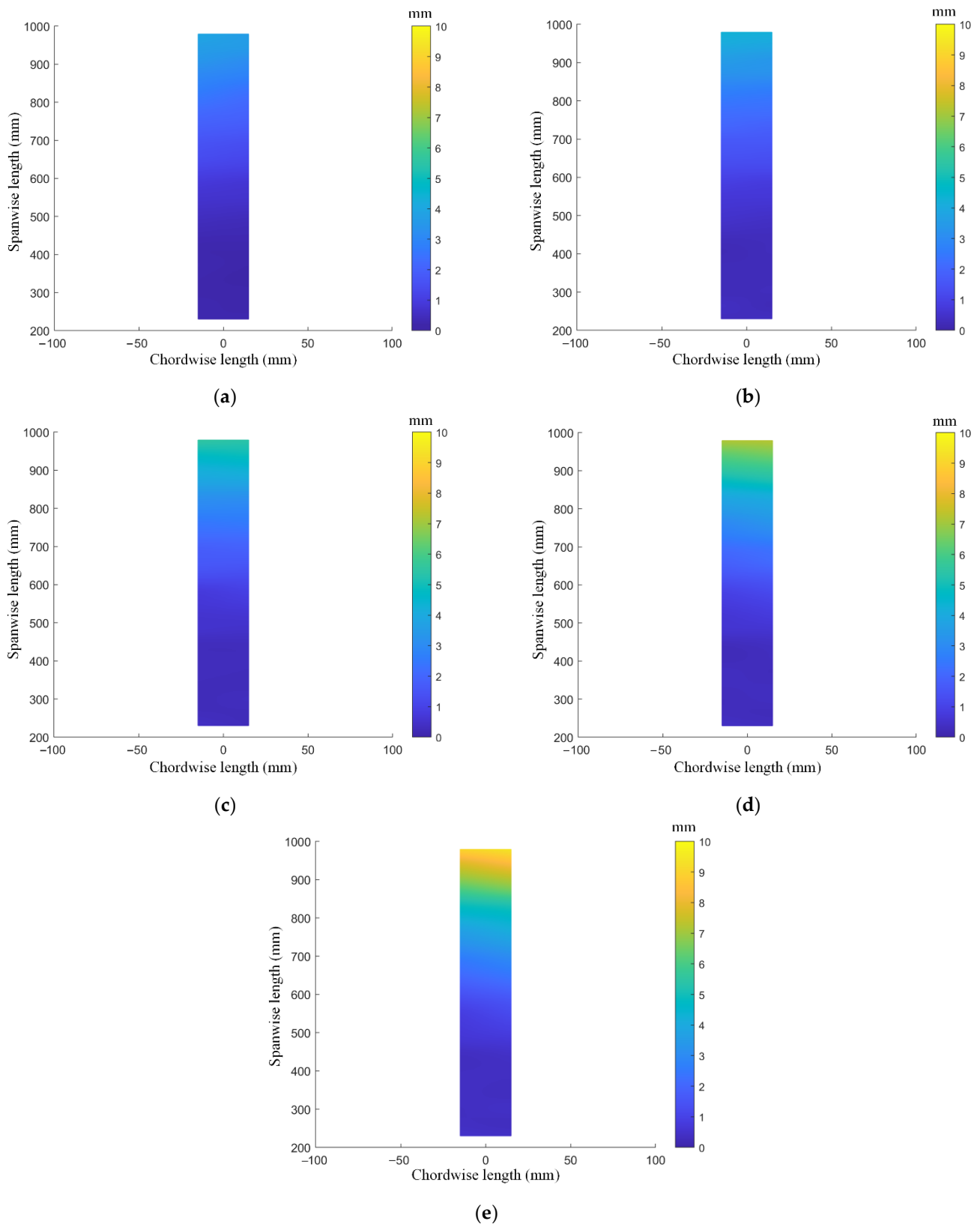


Figure 14. Average deformations of the rotor blade over its full rotating range at the collective pitch angles of (a) $\theta = 0^\circ$, (b) $\theta = 2^\circ$, (c) $\theta = 4^\circ$, (d) $\theta = 6^\circ$ and (e) $\theta = 8^\circ$.

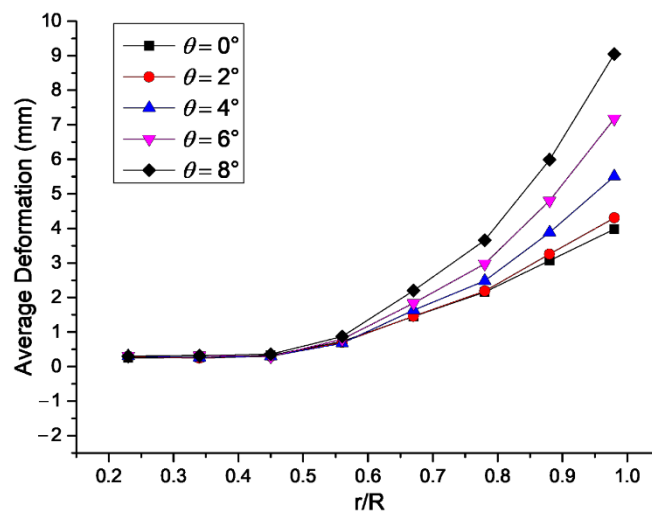


Figure 15. Average deformations at eight radial locations with five collective pitch angles.

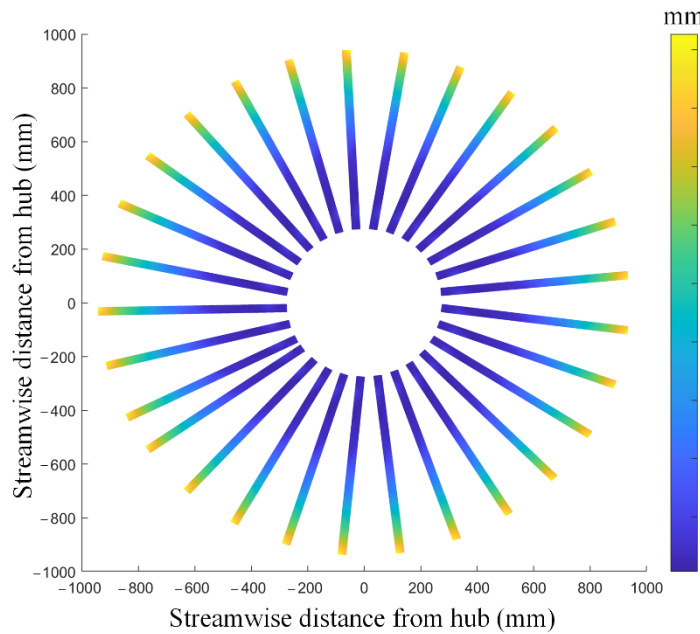


Figure 16. Blade deformations over its full rotating range with the collective pitch angle of $\theta = 8^\circ$.

In the experiments, the actual blade deformation was unknown, thus it was hard to evaluate its measurement accuracy. However, since the spatial distance of any two targets on the rotor hub or the blade were known, the measurement accuracy in current study could be evaluated with the measured three-dimensional distances of them. Table 2 shows the measurement accuracy of different test conditions in the experiments.

Table 2. Measurement accuracy.

θ ($^\circ$)	Accuracy of Hub Targets (mm)	Accuracy of Blade Targets (mm)
0	0.125	0.204
2	0.131	0.251
4	0.143	0.231
6	0.148	0.205
8	0.116	0.233
Average	0.132	0.224

5. Conclusions

In this paper, a photogrammetric system for the full-field deformation measurements of helicopter rotor blades was developed. By detecting and recognizing the targets attached on the rotor hub hat, the dynamic motion of the rotor shaft was tracked, and a unified coordinate system was established on the rotor, where the possible vibration effects caused by the photogrammetric system or the rotor could be avoided effectively. Based on the 3D reconstruction results of the blade targets, the blade displacements and deformations over its full rotating range were further calculated. The photogrammetric system was validated in the wind tunnel test of a 2 m-diameter rotor. The instantaneous locations of the rotor blade at its 30 azimuths under different test conditions were measured. The experimental results agreed with the simulation results quite well.

Author Contributions: Conceptualization, C.Z. and J.M.; methodology, C.Z.; software, J.S. and C.W.; validation, J.S., C.W. and T.Y.; writing—original draft preparation, C.Z.; writing—review and editing, J.M.; visualization, C.W. and T.Y. All authors have read and agreed to the published version of the manuscript.

Funding: This research was funded by the National Natural Science Foundation of China, grant number 52006235.

Data Availability Statement: The data used to support the findings of this study are available from the corresponding author upon request.

Conflicts of Interest: The authors declare no conflict of interest.

References

1. Tourjansky, N.; Szechenyi, E. The measurement of blade deflections—A new implementation of the strain pattern analysis. In Proceedings of the European Rotorcraft Forum, Avignon, France, 15–17 September 1992; ONERA—The French Aerospace Laboratory: Palaiseau, France, 1992.
2. Kufeld, R.M.; Balough, D.L.; Cross, J.L.; Studebaker, K.F.; Jennison, C.D.; Bousman, W.G. Flight testing the UH-60A airloads aircraft. In Proceedings of the Annual Forum of the American Helicopter Society, Washington, DC, USA, 11–13 May 1994.
3. Schmidt, T.; Tyson, J.; Galanulis, K. Full-field dynamic displacement and strain measurement using advanced 3D image correlation photogrammetry: Part I. *Exp. Tech.* **2003**, *27*, 47–50. [[CrossRef](#)]
4. Fleming, G.A.; Gorton, S.A. Measurement of rotorcraft blade deformation using projection moire interferometry. *Shock Vib.* **2000**, *7*, 149–166. [[CrossRef](#)]
5. Fleming, G.A.; Soto, H.L.; South, B.W. Projection moire interferometry for rotorcraft applications: Deformation measurements of active twist rotor blades. In Proceedings of the American Helicopter Society 58th Annual Forum, Montreal, QC, Canada, 11–13 June 2002.
6. Sekula, M. The development and hover test application of a projection moire interferometry blade displacement measurement system. In Proceedings of the American Helicopter Society Annual Forum, Fort Worth, TX, USA, 1–3 May 2012.
7. Schneider, O.; Wall, B.G.V.D.; Pengel, K. HART II blade motion measured by stereo pattern recognition. In Proceedings of the American Helicopter Society Forum, Phoenix, AZ, USA, 6–8 May 2003.
8. Schneider, O.; Wall, B.G.V.D. Final analysis of HART II blade deflection measurements. In Proceedings of the European Rotorcraft Forum, Friedrichshafen, Germany, 16–18 September 2003.
9. Schneider, O. Analysis of SPR measurements from HART II. *Aerosp. Sci. Technol.* **2005**, *9*, 409–420. [[CrossRef](#)]
10. Olson, L.E.; Abrego, A.I.; Barrows, D.A.; Burner, A.W. Blade deflection measurements of a full-scale UH-60A rotor system. In Proceedings of the American Helicopter Society Aeromechanics Specialist Conference, San Francisco, CA, USA, 20–22 January 2010.
11. Abrego, A.I.; Olson, L.E.; Romander, E.A.; Barrows, D.A.; Burner, A.W. Blade displacement measurement technique applied to a full-scale rotor test. In Proceedings of the American Helicopter Society Annual Forum, Fort Worth, TX, USA, 1–3 May 2012.
12. Romander, E.; Meyn, L.; Norman, T.R.; Barrows, D.; Burner, A. Blade motion correlation for the full-scale UH-60A airloads rotor. In Proceedings of the AHS 5th Decennial Aeromechanics Specialists Conference, San Francisco, CA, USA, 22–24 January 2014.
13. Abrego, A.; Meyn, L.; Burner, A.; Barrows, D. Summary of full-scale blade displacement measurements of the UH-60A airloads rotor. In Proceedings of the AHS Technical Meeting on Aeromechanics Design for Vertical Lift, San Francisco, CA, USA, 20–22 January 2016.
14. Straub, F.K.; Anand, V.R.; Lau, B.H.; Birchette, T.S. Wind tunnel test of the SMART active flap rotor. *J. Am. Helicopter Soc.* **2018**, *63*, 1–16. [[CrossRef](#)]
15. Zuo, C.; Ma, J.; Yue, T.; Song, J.; Shi, Z. Blade displacement measurements of helicopter rotor based on stereo vision. In Proceedings of the 18th International Symposium on Flow Visualization, Zurich, Switzerland, 26–29 June 2018.

16. Zuo, C.; Ma, J.; Yue, T.; Song, J.; Wang, X. Displacement and deformation measurements of helicopter rotor blades based on binocular stereo vision. *J. Exp. Fluid Mech.* **2020**, *34*, 87–95.
17. Bernardini, G.; Serafini, J.; Enei, C.; Mattioni, L.; Ficuciello, C.; Vezzari, V. Structural characterization of rotor blades through photogrammetry. *Meas. Sci. Technol.* **2016**, *27*, 065401. [[CrossRef](#)]
18. Sirohi, J.; Lawson, M.S. Measurement of helicopter rotor blade deformation using digital image correlation. *Opt. Eng.* **2012**, *51*, 043603. [[CrossRef](#)]
19. Sicard, J.; Sirohi, J. Measurement of the deformation of an extremely flexible rotor blade using digital image correlation. *Meas. Sci. Technol.* **2013**, *24*, 065203. [[CrossRef](#)]
20. Boden, F.; Stasicki, B.; Szypula, M.; Ruzicka, P.; Tvrdek, Z.; Ludwikowski, K. In-flight measurements of propeller blade deformation on a VUT100 cobra aeroplane using a co-rotating camera system. *Meas. Sci. Technol.* **2016**, *27*, 074013. [[CrossRef](#)]
21. Uehara, D.; Sirohi, J. Full-field optical deformation measurement and operational modal analysis of a flexible rotor blade. *Mech. Syst. Signal Processing* **2019**, *133*, 106265. [[CrossRef](#)]
22. Wei, B.; Liang, J.; Hu, H.; Ren, M.; Yi, H.; Li, J. A videogrammetric system for measuring the full-field blade deformation of a heavy-duty helicopter's Rotating Rotor. *Rev. Sci. Instrum.* **2018**, *89*, 115111. [[CrossRef](#)] [[PubMed](#)]
23. Sousa, P.J.; Barros, F.; Tavares, P.J.; Moreira, P.M. Displacement measurement and shape acquisition of an rc helicopter blade using digital image correlation. *Procedia Struct. Integr.* **2017**, *5*, 1253–1259. [[CrossRef](#)]
24. Sousa, P.J.; Barros, F.; Tavares, P.J.; Moreira, P.M. Digital image correlation displacement measurement of a rotating RC helicopter blade. *Eng. Fail. Anal.* **2018**, *90*, 371–379. [[CrossRef](#)]